First Results from KamLAND: Evidence for Reactor Anti-Neutrino Disappearance

K. Eguchi,[1] S. Enomoto,[1] K. Furuno,[1] J. Goldman,[1] H. Hanada,[1] H. Ikeda,[1] K. Ikeda,[1] K. Inoue,[1] K. Ishihara,[1] W. Itoh,[1] T. Iwamoto,[1] T. Kawaguchi,[1] T. Kawashima,[1] H. Kinoshita,[1] Y. Kishimoto,[1] M. Koga,[1] Y. Koseki,[1] T. Maeda,[1] T. Mitsui,[1] M. Motoki,[1] K. Nakajima,[1] M. Nakajima,[1] T. Nakajima,[1] H. Ogawa,[1] K. Owada,[1] T. Sakabe,[1] I. Shimizu,[1] J. Shirai,[1] F. Suekane,[1] A. Suzuki,[1] K. Tada,[1] O. Tajima,[1] T. Takayama,[1] K. Tamae,[1] H. Watanabe,[1] J. Busenitz,[2] Ž. Djurčić,[2] K. McKinny,[2] D-M. Mei,[2] A. Piepke,[2] E. Yakushev,[2] B.E. Berger,[3] Y.D. Chan,[3] M.P. Decowski,[3] D.A. Dwyer,[3] S.J. Freedman,[3] Y. Fu,[3] B.K. Fujikawa,[3] K.M. Heeger,[3] K.T. Lesko,[3] K.-B. Luk,[3] H. Murayama,[3] D.R. Nygren,[3] C.E. Okada,[3] A.W.P. Poon,[3] H.M. Steiner,[3] L.A. Winslow,[3] G.A. Horton-Smith,[4] R.D. McKeown,[4] J. Ritter,[4] B. Tipton,[4] P. Vogel,[4] C.E. Lane,[5] T. Miletic,[5] P.W. Gorham,[6] G. Guillian,[6] J.G. Learned,[6] J. Maricic,[6] S. Matsuno,[6] S. Pakvasa,[6] S. Dazeley,[7] S. Hatakeyama,[7] M. Murakami,[7] R.C. Svoboda,[7] B.D. Dieterle,[8] M. DiMauro,[8] J. Detwiler,[9] G. Gratta,[9] K. Ishii,[9] N. Tolich,[9] Y. Uchida,[9] M. Batygov,[10] W. Bugg,[10] H. Cohn,[10] Y. Efremenko,[10] Y. Kamyshkov,[10] A. Kozlov,[10] Y. Nakamura,[10] L. De Braeckeleer,[11] C.R. Gould,[11] H.J. Karwowski,[11] D.M. Markoff,[11] J.A. Messimore,[11] K. Nakamura,[11] R.M. Rohm,[11] W. Tornow,[11] A.R. Young,[11] and Y-F. Wang[12]

(KamLAND Collaboration)

[1] *Research Center for Neutrino Science, Tohoku University, Sendai 980-8578, Japan*
[2] *Department of Physics and Astronomy, University of Alabama, Tuscaloosa, Alabama 35487, USA*
[3] *Physics Department, University of California at Berkeley and Lawrence Berkeley National Laboratory, Berkeley, California 94720, USA*
[4] *W. K. Kellogg Radiation Laboratory, California Institute of Technology, Pasadena, California 91125, USA*
[5] *Physics Department, Drexel University, Philadelphia, Pennsylvania 19104, USA*
[6] *Department of Physics and Astronomy, University of Hawaii at Manoa, Honolulu, Hawaii 96822, USA*
[7] *Department of Physics and Astronomy, Louisiana State University, Baton Rouge, Louisiana 70803, USA*
[8] *Physics Department, University of New Mexico, Albuquerque, New Mexico 87131, USA*
[9] *Physics Department, Stanford University, Stanford, California 94305, USA*
[10] *Department of Physics and Astronomy, University of Tennessee, Knoxville, Tennessee 37996, USA*
[11] *Triangle Universities Nuclear Laboratory, Durham, North Carolina 27708, USA and Physics Departments at Duke University, North Carolina State University, and the University of North Carolina at Chapel Hill*
[12] *Institute of High Energy Physics, Beijing 100039, People's Republic of China*

(Dated: December 9, 2002)

KamLAND has been used to measure the flux of $\bar{\nu}_e$'s from distant nuclear reactors. In an exposure of 162 ton·yr (145.1 days) the ratio of the number of observed inverse β-decay events to the expected number of events without disappearance is $0.611 \pm 0.085(\text{stat}) \pm 0.041(\text{syst})$ for $\bar{\nu}_e$ energies > 3.4 MeV. The deficit of events is inconsistent with the expected rate for standard $\bar{\nu}_e$ propagation at the 99.95% confidence level. In the context of two-flavor neutrino oscillations with CPT invariance, these results exclude all oscillation solutions but the 'Large Mixing Angle' solution to the solar neutrino problem using reactor $\bar{\nu}_e$ sources.

PACS numbers: 14.60.Pq, 26.65.+t, 28.50.Hw, 91.65.Dt

arXiv:hep-ex/0212021v1 9 Dec 2002

The primary goal of the Kamioka Liquid scintillator Anti-Neutrino Detector (KamLAND) experiment [1] is a search for the oscillation of $\bar{\nu}_e$'s emitted from distant power reactors. The long baseline, typically 180 km, enables KamLAND to address the oscillation solution of the 'solar neutrino problem' using reactor anti-neutrinos under laboratory conditions. The inverse β-decay reaction, $\bar{\nu}_e + p \rightarrow e^+ + n$, is utilized to detect $\bar{\nu}_e$'s with energies above 1.8 MeV in liquid scintillator (LS) [2]. The detection of the e^+ and the 2.2 MeV γ-ray from neutron capture on a proton in delayed coincidence is a powerful tool for reducing background. This letter presents the first results from an analysis of 162 ton·yr of the reactor $\bar{\nu}_e$ data.

KamLAND is located at the site of the earlier Kamiokande [3], with an average rock overburden of 2,700 m.w.e. resulting in 0.34 Hz of cosmic-ray muons in the detector volume. As shown in Fig. 1, the neutrino detector/target is 1 kton of ultra-pure LS contained in a 13-m-diameter spherical balloon made of 135-μm-thick transparent nylon/EVOH (Ethylene vinyl alcohol copolymer) composite film. The balloon is supported and constrained by a network of kevlar ropes. The LS is 80% dodecane, 20% pseudocumene (1,2,4-Trimethylbenzene), and 1.52 g/liter of PPO (2,5-Diphenyloxazole) as a fluor. A buffer of dodecane and isoparaffin oils between the balloon and an 18-m-diameter spherical stainless-steel containment vessel shields the LS from external radiation. During the filling procedure a water extraction and nitrogen bubbling method [4], optimized for KamLAND, was used to purify the LS and buffer oil; PPO prepurification and dust removal were especially important.

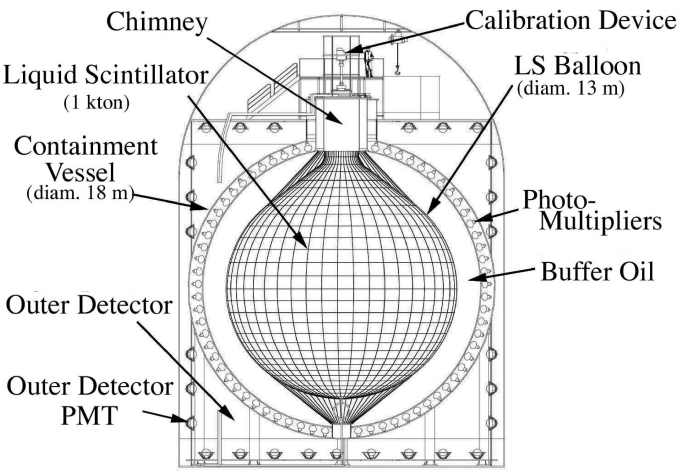

FIG. 1: Schematic diagram of the KamLAND detector.

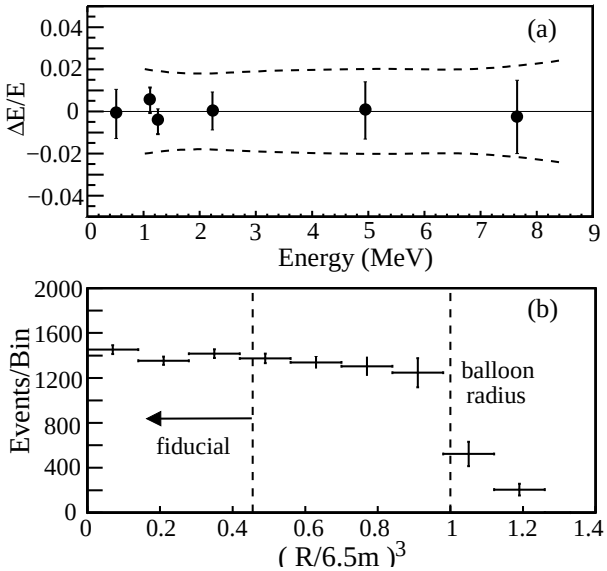

FIG. 2: (a) The fractional difference of the reconstructed average γ energies and average source energies. The dashed line shows the systematic error. (b) The R^3 vertex distribution of 2.2 MeV neutron capture γ's.

The specific gravity of the buffer oil is adjusted to be 0.04% lower than that of the LS. An array of 1,879 photomultiplier tubes (PMTs), mounted on the inner surface of the containment vessel, completes the inner detector (ID) system. This array includes 1,325 specially developed fast PMTs with 17-inch-diameter photocathodes and 554 older Kamiokande 20-inch PMTs [5]. While the total photo-cathode coverage is 34%, only the 17-inch PMTs corresponding to 22% coverage are used for the analysis in this letter. A 3-mm-thick acrylic barrier at 16.6-m diameter helps prevent radon emanating from PMT glass from entering the LS. The containment vessel is surrounded by a 3.2 kton water-Cherenkov detector with 225 20-inch PMTs. This outer detector (OD) absorbs γ-rays and neutrons from the surrounding rock and provides a tag for cosmic-ray muons. The primary ID trigger threshold is set at 200 PMT hits, corresponding to about 0.7 MeV. This threshold is lowered to 120 hits for 1 msec after the primary trigger to observe lower energy delayed activity. The OD trigger threshold is set to provide $> 99\%$ tagging efficiency.

The inner detector is calibrated with γ-ray sources of ^{68}Ge, ^{65}Zn, ^{60}Co, and Am-Be, deployed at various positions along the vertical axis. These sources provide calibration energies in the 0.5 to 7.6 MeV region. Energy measurements are based on the number of detected photoelectrons (p.e.) with corrections for PMT gain variation, solid angle, the density of PMTs, shadowing by suspension ropes, and light transparencies of the LS and buffer oil. At the center, about 300 p.e. per MeV are observed. Fig. 2 (a) shows the fractional deviation of the reconstructed energies from the source energies. The ^{68}Ge and ^{60}Co sources emit two coincident γ-rays and are plotted at an average energy in Fig. 2 (a). The observed energy resolution is $\sim 7.5\%/\sqrt{E(\mathrm{MeV})}$.

The energy calibration is augmented with studies of ^{40}K and ^{208}Tl (which are contaminants in the detector), Bi-Po sequential decays, the spallation products ^{12}B and ^{12}N, and γ's from thermal neutron captures on protons and ^{12}C. The reconstructed energy varies by less than 0.5% within the 10-m-diameter fiducial volume; local variations near the chimney region are about 1.6%. The energy scale exhibits less than 0.6% variation in time during the entire data run. Corrections for quenching and Cherenkov light production are included, and contribute to the systematic error in Fig. 2 (a). The estimated systematic error for the energy scale is 1.9% at the 2.6 MeV energy threshold which corresponds to a 2.1% uncertainty in the detected neutrino rate. Correlated decays from Bi-Po and ^{8}He/^{9}Li yield energies between 0.6 MeV and $\sim$15 MeV and are used to extend the range of the energy calibration.

The source positions are reconstructed from the relative times of PMT hits. Energy-dependent radial adjustments are used to reproduce the known source positions to $\sim$5 cm; the typical position reconstruction resolution is 25 cm. Vertex reconstruction performance throughout the LS volume is verified by reproducing the uniform distribution of 2.2 MeV capture γ's from spallation neutrons, as shown in Fig. 2 (b).

The data presented in this letter were obtained during a period from March 4 through October 6, 2002. In total we collected 370 million events in 145.1 days of live time, corresponding to an average trigger rate of $\simeq$30 Hz. Events with fewer than 10,000 p.e. ($\sim$30 MeV) and no prompt OD veto signal are classified as 'reactor $\bar{\nu}_e$ candidates'; more energetic events are treated as 'muon candidates.'

The criteria for selection of $\bar{\nu}_e$ events are (1) a fiducial volume cut ($R < 5$ m), (2) a time correlation cut ($0.5\ \mu\mathrm{sec} < \Delta T < 660\ \mu\mathrm{sec}$), (3) a vertex correlation

cut ($\Delta R < 1.6$ m), (4) a delayed energy window cut (1.8 MeV $< E_{delay} <$ 2.6 MeV), and (5) a cut on the delayed vertex position requiring it to be more than 1.2 m from the central vertical axis (to eliminate background from thermometers deployed in this region to monitor LS temperature). The overall efficiency associated with criteria (2)-(5) combined with the effect of (1) on the delayedvertex is $(78.3 \pm 1.6)\%$.

Positrons annihilate in the LS and the detected energy includes the kinetic energy plus twice the electron rest mass; thus e^+ from $\bar{\nu}_e$ events produce $E_{prompt} = E_{\bar{\nu}_e} - \bar{E}_n - 0.8$ MeV, where $\bar{E}_n$ is the average neutron recoil energy. Anti-neutrinos emitted by ^{238}U and ^{232}Th decays in the Earth, 'geo-neutrinos' ($\bar{\nu}_{geo}$), contribute low-energy events with $E_{prompt} < 2.49$ MeV. For example, model Ia of $\bar{\nu}_{geo}$ in [6] predicts about 9 $\bar{\nu}_{geo}$ events in our data set. However the abundances of U and Th and their distributions in the Earth are not well known. To avoid ambiguities from $\bar{\nu}_{geo}$'s we employ (6) a prompt energy cut, $E_{prompt} > 2.6$ MeV in the present analysis.

Low-energy γ-rays from ^{208}Tl ($\simeq$3 Hz) entering from outside the balloon are potential sources of background in the range up to 3 MeV and are strongly suppressed by the fiducial volume cut (1). The fiducial volume is estimated using the uniform distribution of spallation neutron capture events shown in Fig. 2 (b). The ratio of these events in the fiducial volume to those in the total volume agrees with the geometric fiducial fraction to within 4.06%. The same method is used for higher energy events, ^{12}N, ^{12}B β's following muon spallation, and agrees within 3.5%. Accounting for uncertainty in the LS total mass of 2.1%, we estimate the total systematic uncertainty of the fiducial volume to be 4.6%. The density of the LS is 0.780 g/cm^3 at 11.5°C; the hydrogen-to-carbon ratio is computed from the LS components to be 1.969 and was verified by elemental analysis ($\pm$2%). The specific gravity of the LS is measured to 0.01% precision using a commercial density meter, and we assign an additional 0.1% systematic error due to the uncertainty in the LS temperature. The 408 ton fiducial mass thus contains 3.46×10^{31} free target protons.

The trigger efficiency was determined to be 99.98% using LED light sources. The combined efficiency of the electronics, data acquisition, and event reconstruction was carefully studied using time distributions of uncorrelated events from calibration γ sources. We find that this combined efficiency is greater than 99.98%. The vertex fitter yields $>$ 99.9% efficiency within 2 m of known source positions. Using calibrated ^{60}Co and ^{65}Zn sources, the overall efficiency was verified to within the 3% uncertainty in source strengths. The detection efficiency of delayed events from the Am-Be source (4.4 MeV prompt γ and 2.2 MeV delayed neutron capture γ within 1.6 m) was verified with 1% uncertainty.

From studies of Bi-Po sequential decays, the equilibrium concentrations of ^{238}U and ^{232}Th in the LS are estimated to be $(3.5 \pm 0.5) \times 10^{-18}$ g/g and $(5.2 \pm 0.8) \times 10^{-17}$ g/g, respectively. The observed background energy spectrum constrains the ^{40}K contamination to be less than 2.7×10^{-16} g/g. The accidental background, obtained from the observed flat distribution in the delayed time window 0.020-20 sec, is 0.0086 ± 0.0005 events for the present data set.

TABLE I: Background summary.

Background	Number of events
Accidental	0.0086 ± 0.0005
^{9}Li/^{8}He	0.94 ± 0.85
Fast neutron	< 0.5
Total B.G. events	0.95 ± 0.99

At higher energies, the background is dominated by spallation products from energetic muons. We observe $\sim$3,000 neutron events/day/kton. We also expect $\sim$1,300 events/day/kton [7] for various unstable products.

Single neutrons are efficiently suppressed by a 2-msec veto following a muon, but care is required to avoid neutrons which mimic the $\bar{\nu}_e$ delayed coincidence signal. Most fast neutrons are produced by energetic muons which pass through both the OD and the surrounding rock. This background is evaluated by detecting delayed coincidence events with a prompt signal associated with a muon detected only by the OD. As expected, a clear concentration of events near the balloon edge is observed. The expected background inside the fiducial volume is estimated by extrapolating the vertex position distribution and considering an OD reconstruction efficiency of 92%. To estimate the number of background events due to neutrons from the surrounding rock, the OD-associated rate is scaled by the relative neutron production and neutron shielding properties of the relevant materials. We estimate that the total fast neutron background is less than 0.5 events for the entire data set.

Most radioactive spallation products simply beta decay, and are effectively suppressed by requiring a delayed neutron signal. Delayed neutron emitters like ^{8}He ($T_{1/2} = 119$ msec) and ^{9}Li (178 msec) are eliminated by two time/geometry cuts: (a) a 2-sec veto is applied for the entire fiducial volume following a showering muon (those with more than 10^6 p.e., $\sim$3 GeV, extra energy deposition), (b) for the remaining muons, delayed events within 2 sec and 3 m from a muon track are rejected. The efficiency of these cuts is calculated from the observed correlation of spallation neutrons with muon tracks. The remaining ^{8}He and ^{9}Li background is estimated to be

TABLE II: Estimated systematic uncertainties (%).

Total LS mass	2.1	Reactor power	2.0
Fiducial mass ratio	4.1	Fuel composition	1.0
Energy threshold	2.1	Time lag	0.28
Efficiency of cuts	2.1	ν spectra [8]	2.5
Live time	0.07	Cross section [11]	0.2
Total systematic error			6.4%

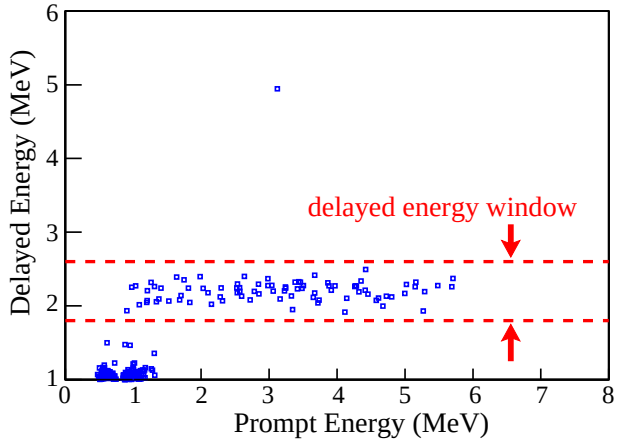

FIG. 3: Distribution of $\bar{\nu}_e$ candidates with fiducial volume cut, time, vertex correlation, and spallation cuts applied. The prompt energy corresponds to the positron and the delayed energy to the captured neutron. The events within the horizontal lines bracketing the delayed energy of 2.2 MeV are due to thermal neutron capture on protons. The events with prompt energy below ∼0.7 MeV are obtained from the delayed trigger. The one event with delayed energy near 4.95 MeV is consistent with theexpected 0.54% fraction from ^{12}C(n,γ).

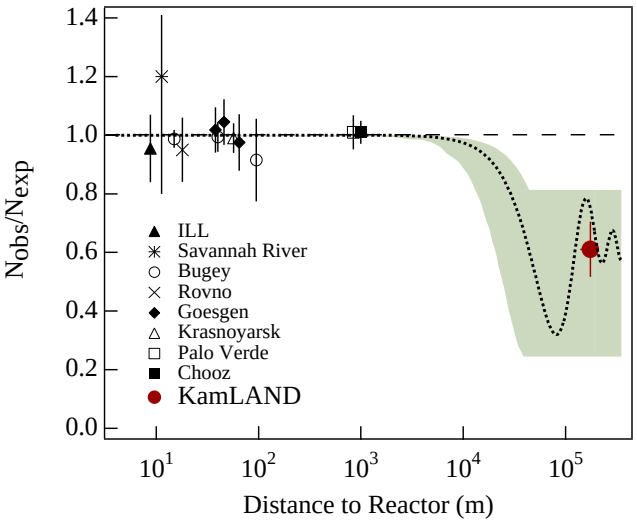

FIG. 4: The ratio of measured to expected $\bar{\nu}_e$ flux from reactor experiments [12]. The solid dot is the KamLAND point plotted at a flux-weighted average distance (the dot size is indicative of the spread in reactor distances). The shaded region indicates the range of flux predictions corresponding to the 95% C.L. LMA region found in a global analysis of the solar neutrino data [13]. The dotted curve corresponds to $\sin^2 2\theta = 0.833$ and $\Delta m^2 = 5.5 \times 10^{-5}$ eV^2 [13] and is representative of recent best-fit LMA predictions while the dashed curve shows the case of small mixing angles (or no oscillation).

0.94 ± 0.85. The dead time due to the spallation cuts is 11.4%. This method is checked by exploiting the time distribution of the events after a detected muon to separate the short-lived spallation-produced activities from $\bar{\nu}_e$ candidates. The uncorrelated $\bar{\nu}_e$ event distribution has a characteristic time constant of $1/R_\mu \simeq 3$ sec, where R_μ is the incident muon rate. Spallation products have a much shorter time constant (∼0.2 sec). These methods agree to 3% accuracy. As shown in Table I the total number of expected background events is 0.95 ± 0.99, where the fast neutron contribution is included in the error estimate.

Instantaneous thermal power generation, burn-up and fuel exchange records for all Japanese commercial power reactors are provided by the power companies. The time dependence of the thermal power generation data is checked by comparison with the independent records of electric power generation. The fission rate for each fissile element is calculated from these data, resulting in a systematic uncertainty in the $\bar{\nu}_e$ flux of less than 1%. Averaged over the present live-time period, the relative fission yields from the various fuel components are ^{235}U : ^{238}U : ^{239}Pu : ^{241}Pu = 0.568 : 0.078 : 0.297 : 0.057. The $\bar{\nu}_e$ spectrum per fission and its error (2.48%) are taken from the literature [8]. These neutrino spectra have been tested to a few percent accuracy in previous short-baseline reactor $\bar{\nu}_e$ experiments [2, 9]. The finite β-decay lifetimes of fission products introduce an additional uncertainty of 0.28% to the $\bar{\nu}_e$ flux; this is estimated from the difference of the total $\bar{\nu}_e$ yield associated with shifting the run time by one day. The contribution to the $\bar{\nu}_e$ flux from Korean reactors is estimated to be (2.46 ± 0.25)% from the reported electric power generation rates. Other reactors around the world give an average (0.70 ± 0.35)% contribution, which is estimated by using reactor specifications from the International Nuclear Safety Center [10]. The uncertainties for the event rate calculation are summarized in Table II. The errors from reactors outside Japan are included in the table under 'Reactor Power'.

Although the anti-neutrino flux at the location of KamLAND is due to many nuclear reactors at a variety of distances, the $\bar{\nu}_e$ flux is actually dominated by a few reactors at an average distance of ∼180 km. More than 79% of the computed flux arises from 26 reactors within the distance range 138-214 km. One reactor at 88 km contributes an additional 6.7% to the flux and the other reactors are more than 295 km away. This relatively narrow band of distances implies that for some oscillation parameters KamLAND can observe a distortion of the $\bar{\nu}_e$ energy spectrum.

The flux of anti-neutrinos from a reactor a distance L from KamLAND is approximately proportional to the thermal power flux $P_{th}/4\pi L^2$, where P_{th} is the reactor thermal power. The integrated total thermal power flux during the measurement live time is 254 Joule/cm^2. The systematic error assigned to the thermal power is conservatively taken as 2% from the regulatory specification for safe reactor operation. The corresponding expected number of reactor neutrino events (in the absence of neutrino oscillations) in the fiducial volume for this data set is 86.8 ± 5.6.

The distribution of prompt and delayed energies for

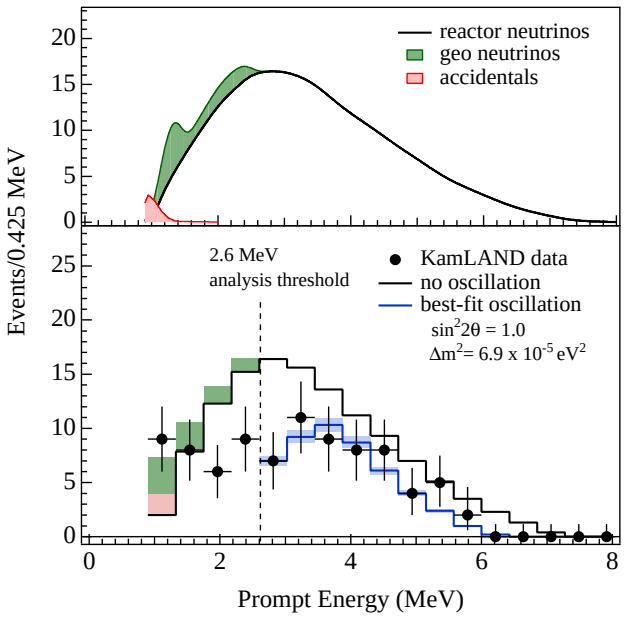

FIG. 5: Upper panel: Expected reactor $\bar{\nu}_e$ energy spectrum with contributions of $\bar{\nu}_{geo}$ (model Ia of [6]) and accidental backround. Lower panel: Energy spectrum of the observed prompt events (solid circles with error bars), along with the expected no oscillation spectrum (upper histogram, with $\bar{\nu}_{geo}$ and accidentals shown) and best fit (lower histogram) including neutrino oscillations. The shaded band indicates the systematic error in the best-fit spectrum. The vertical dashed line corresponds to the analysis threshold at 2.6 MeV.

the present sample before the energy cuts are applied is shown in Fig. 3. A clear cluster of events from the 2.2 MeV capture γ's is observed. One event with delayed energy around 5 MeV is consistent with a thermal neutron capture γ on ^{12}C. The space-time correlation of the prompt and delayed events is in good agreement with expectations, and the observed mean neutron capture time is 188 ± 23 μsec. After applying the prompt and delayed energy cuts, 54 events remain as the final sample. The ratio of the number of observed reactor $\bar{\nu}_e$ events to that expected in the absence of neutrino oscillations is

$$\frac{N_{obs} - N_{BG}}{N_{expected}} = 0.611 \pm 0.085(\mathrm{stat}) \pm 0.041(\mathrm{syst}).$$

The probability that the KamLAND result is consistent with the no disappearance hypothesis is less than 0.05%. Fig. 4 shows the ratio of measured to expected flux for KamLAND as well as previous reactor experiments as a function of the average distance from the source.

The observed prompt energy spectrum is shown in Fig. 5. The expected positron spectrum with no oscillations and the best fit with two-flavor neutrino oscillations above the 2.6 MeV threshold are shown. A clear deficit of events is observed. The measured spectrum is consistent (93% confidence) with a distorted spectrum shape as expected from neutrino oscillations, but a renormalized no-oscillation shape is also consistent at 53% confidence.

The neutrino oscillation parameter region for two-neutrino mixing is shown in Fig. 6. The dark shaded area is the LMA region at 95% C.L. derived from [13]. The shaded region outside the solid line is excluded at 95% C.L. from the rate analysis with $\Delta\chi^2 \geq 3.84$ and

$$\chi^2 = \frac{(0.611 - R(\sin^2 2\theta, \Delta m^2))^2}{0.085^2 + 0.041^2}.$$

Here, $R(\sin^2 2\theta, \Delta m^2)$ is the expected ratio with the oscillation parameters.

The spectrum of the final event sample is then analyzed with a maximum likelihood method to obtain the optimum set of oscillation parameters with the following χ^2 definition:

$$\begin{aligned}\chi^2 \;=\; & \chi^2_{\mathrm{rate}}(\sin^2 2\theta, \Delta m^2, N_{\mathrm{BG1\sim2}}, \alpha_{1\sim4}) \\ & -2\log L_{\mathrm{shape}}(\sin^2 2\theta, \Delta m^2, N_{\mathrm{BG1\sim2}}, \alpha_{1\sim4}) \\ & +\chi^2_{\mathrm{BG}}(N_{\mathrm{BG1\sim2}}) + \chi^2_{\mathrm{distortion}}(\alpha_{1\sim4}),\end{aligned}$$

where L_{shape} is the likelihood function of the spectrum including deformations from various parameters. $N_{\mathrm{BG1\sim2}}$ are the estimated number of ^{9}Li and ^{8}He backgrounds and $\alpha_{1\sim4}$ are the parameters for the shape deformation coming from energy scale, resolution, $\bar{\nu}_e$ spectrum and fiducial volume. These parameters are varied to minimize the χ^2 at each pair of $[\Delta m^2, \sin^2\theta]$ with a bound from $\chi^2_{\mathrm{BG}}(N_{\mathrm{BG1\sim2}})$ and $\chi^2_{\mathrm{distortion}}(\alpha_{1\sim4})$. The best fit to the KamLAND data in the physical region yields $\sin^2 2\theta = 1.0$ and $\Delta m^2 = 6.9 \times 10^{-5}$ eV^2 while the global minimum occurs slightly outside of the physical region at $\sin^2 2\theta = 1.01$ with the same Δm^2. These numbers can be compared to the best fit LMA values of $\sin^2 2\theta = 0.833$ and $\Delta m^2 = 5.5 \times 10^{-5}$ eV^2 from [13]. The 95% C.L. allowed regions from the spectrum shape analysis are shown in Fig. 6. The allowed regions displayed for KamLAND correspond to $0 < \theta < \frac{\pi}{4}$ consistent with the solar LMA solution, but for KamLAND the allowed regions in $\frac{\pi}{4} < \theta < \frac{\pi}{2}$ are identical [14].

Another spectral shape analysis is performed with a lower prompt energy threshold of 0.9 MeV in order to check the stability of the above result and study the sensitivity to $\bar{\nu}_{geo}$. With this threshold, the total background is estimated to be 2.91 ± 1.12 events, most of which come from accidental and spallation events. The systematic error is 6.0%, which is smaller than that for the final event sample due to the absence of an energy threshold effect. When the maximum likelihood is calculated, the $\bar{\nu}_{geo}$ fluxes from ^{238}U and ^{232}Th are treated as free parameters. The best fit in this analysis yields $\sin^2 2\theta = 0.91$ and $\Delta m^2 = 6.9 \times 10^{-5}$eV^2. These results and the allowed region of the oscillation parameters are in good agreement with the results obtained above. The numbers of $\bar{\nu}_{geo}$ events for the best fit are 4 for ^{238}U and 5 for ^{232}Th, which corresponds to $\sim$40 TW radiogenic heat generation according to model Ia in [6]. However, for the same model, $\bar{\nu}_{geo}$ production powers from 0 to 110 TW

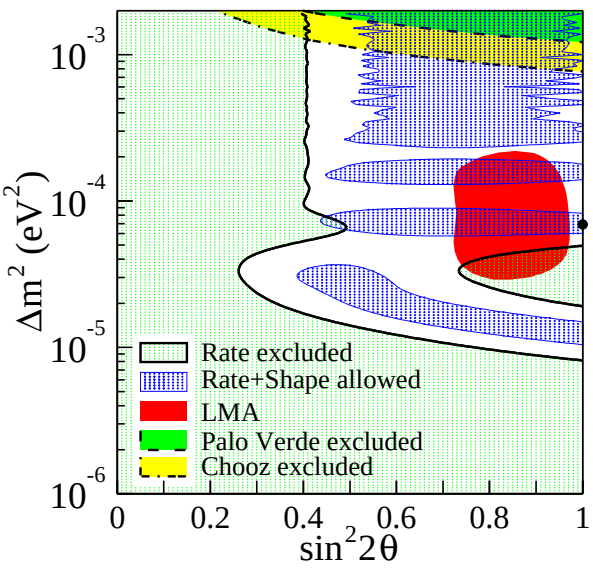

FIG. 6: Excluded regions of neutrino oscillation parameters for the rateanalysis and allowed regions for the combined rate and shape analysis from KamLAND at 95% C.L. At the top are the 95% C.L. excluded region from CHOOZ [15] and Palo Verde [16] experiments, respectively. The 95% C.L. allowed region of the 'Large Mixing Angle' (LMA) solution of solar neutrino experiments [13] is also shown. The thick dot indicates the best fit to the KamLAND data in the physical region: $\sin^2 2\theta = 1.0$ and $\Delta m^2 = 6.9 \times 10^{-5}\mathrm{eV}^2$. All regions look identical under $\theta \leftrightarrow (\pi/2 - \theta)$ except for the LMA region.

are still allowed at 95% C.L. with the same oscillation parameters.

If three neutrino generations are considered, the $\bar{\nu}_e$ survival probability depends on two mixing angles θ_{12} and θ_{13}. In the region close to the best fit KamLAND solution the survival probability is, to a very good approximation, given by

$$P(\bar{\nu}_e \to \bar{\nu}_e) \cong \cos^4\theta_{13}\left[1 - \sin^2 2\theta_{12}\sin^2\frac{\Delta m^2_{12}L}{4E_\nu}\right],$$

with $\Delta m_{12} \cong \Delta m^2$ from the 2-flavor analysis above. The CHOOZ experiment [15] established an upper limit of $\sin^2 2\theta_{13} < 0.15$, or $\cos^4\theta_{13} \geq 0.92$. The best fit KamLAND result would correspond approximately to $0.86 < \sin^2 2\theta_{12} < 1.0$.

In summary KamLAND has used measurements at large distances (∼180 km) to demonstrate, for the first time, reactor $\bar{\nu}_e$ disappearance at a high confidence level (99.95%). Since one expects a negligible reduction of $\bar{\nu}_e$ flux from the SMA, LOW and VAC solar neutrino solutions, the LMA region is the only remaining oscillation solution consistent with the KamLAND result and CPT invariance. The allowed LMA region is further reduced by these results. Future measurements with greater statistical precision and reduced systematic errors will enable KamLAND to provide a high-precision measurement of the neutrino oscillation parameters.

The KamLAND experiment is supported by the COE program of Japanese Ministry of Education, Culture, Sports, Science and Technology, and funding from the United States Department of Energy. The reactor data are provided by courtesy of the following electric associations in Japan; Hokkaido, Tohoku, Tokyo, Hokuriku, Chubu, Kansai, Chugoku, Shikoku and Kyushu Electric Power Companies, Japan Atomic Power Co. and Japan Nuclear Cycle Development Institute. Kamioka Mining and Smelting Company has provided service for activities in the mine.

[1] A. Suzuki, Talk at the XVIII International Conference on Neutrino Physics and Astrophysics, Takayama, Japan, (1998), and its proceedings. http://www.awa.tohoku.ac.jp/KamLAND/
[2] For a recent comprehensive review of reactor neutrino oscillation experiments, see C. Bemporad, G. Gratta, and P. Vogel, Rev. Mod. Phys. **74**, 297 (2002).
[3] K. S. Hirata *et al.*, Phys. Rev. **D38**, 448 (1988).
[4] J. B. Benziger et al., Nucl. Instr. Meth. **A417**, 278 (1998).
[5] H. Kume *et al.*, Nucl. Instr. and Meth. **205** 443 (1986).
[6] R. S. Raghavan, S. Schoenert, S. Enomoto, J. Shirai, F. Suekane and A. Suzuki, Phys. Rev. Lett. **80**, 635 (1998).
[7] T. Hagner *et al.*, Astropart. Phys. **14** 33 (2000).
[8] ^{235}U : K. Schreckenbach *et al.*, Phys. Lett. **B160**, 325 (1985); ^{239,241}Pu : A. A. Hahn *et al.*, Phys. Lett. **B218**, 365 (1989); ^{238}U : P. Vogel *et al.*, Phys. Rev. **C24**, 1543 (1981).
[9] B. Achkar *et al.*, Phys. Lett. **B374**, 243 (1996), G. Zacek *et al.*, Phys. Rev. **D34**, 2621 (1986).
[10] http://www.insc.anl.gov/
[11] P. Vogel and J. F. Beacom, Phys. Rev. **D60**, 053003 (1999); Outer radiative correction from A. Kurylov, M. J. Ramsey-Musolf and P. Vogel, hep-ph/0211306.
[12] Particle Data Group, Phys. Rev. **D66**, 010001-406 (2002).
[13] G. L. Fogli *et al.*, Phys. Rev. **D66**, 053010 (2002).
[14] A. de Gouvea, A. Friedland, H. Murayama, Phys. Lett. **B490**, 125-130 (2000).
[15] M. Apollonio *et al.*, Phys. Lett. **B466**, 415 (1999).
[16] F. Boehm *et al.*, Phys. Rev. **D64**, 112001 (2001).